Bioactive Materials 9 (2022) 397–410

Contents lists available at ScienceDirect

Bioactive Materials

journal homepage: www.keaipublishing.com/en/journals/bioactive-materials

Uptake of oxidative stress-mediated extracellular vesicles by vascular endothelial cells under low magnitude shear stress

Xian Qin [a,1], Kun Zhang [a,1], Juhui Qiu [a,**,1], Nan Wang [b], Kai Qu [a], Yuliang Cui [a], Junli Huang [a], Li Luo [a], Yuan Zhong [a], Tian Tian [a], Wei Wu [a], Yi Wang [a,***], Guixue Wang [a,*]

[a] Key Laboratory for Biorheological Science and Technology of Ministry of Education, State and Local Joint Engineering Laboratory for Vascular Implants, Bioengineering College of Chongqing University, Chongqing, 400030, China
[b] The Nanoscience Centre, University of Cambridge, Cambridge, CB3 0FF, UK

ARTICLE INFO

Keywords:
Extracellular vesicles (EVs)
Blood flow shear stress
Endothelial cell uptake
Nanoparticles
Oxidative stress

ABSTRACT

Extracellular vesicles (EVs) are increasingly used as delivery vehicles for drugs and bioactive molecules, which usually require intravascular administration. The endothelial cells covering the inner surface of blood vessels are susceptible to the shear stress of blood flow. Few studies demonstrate the interplay of red blood cell-derived EVs (RBCEVs) and endothelial cells. Thus, the phagocytosis of EVs by vascular endothelial cells during blood flow needs to be elucidated. In this study, red blood cell-derived extracellular vesicles (RBCEVs) were constructed to investigate endothelial cell phagocytosis *in vitro* and animal models. Results showed that low magnitude shear stress including low shear stress (LSS) and oscillatory shear stress (OSS) could promote the uptake of RBCEVs by endothelial cells *in vitro*. In addition, in zebrafish and mouse models, RBCEVs tend to be internalized by endothelial cells under LSS or OSS. Moreover, RBCEVs are easily engulfed by endothelial cells in atherosclerotic plaques exposed to LSS or OSS. In terms of mechanism, oxidative stress induced by LSS is part of the reason for the increased uptake of endothelial cells. Overall, this study shows that vascular endothelial cells can easily engulf EVs in areas of low magnitude shear stress, which will provide a theoretical basis for the development and utilization of EVs-based nano-drug delivery systems *in vivo*.

1. Introduction

Nanoparticles are a promising platform for delivering therapeutic molecules directly to the disease site and preventing off-target organ toxicity [1–4]. Therapeutic nanoparticles commonly require intravascular administration, by which nanoparticles will enter the bloodstream, circulate throughout the body, and extravasate out of the blood vessel into the disease site to deliver their cargo [5,6]. As nanoparticles travel in the blood, they pass around the bends and bulges of vessels and contact cells or tissues. In this process, they will experience hemodynamic forces that result in locally high nanoparticle accumulation in some areas and subsequently differential toxicity and efficacy of diagnostics and therapeutics.

A previous study has shown that flow shear stress and velocity are critical factors for drug delivery of nanoparticles travelling in the blood vascular system [7]. Nanoparticles are prone to accumulate in the bifurcation and oscillation regions of blood vessels, especially those near the inner wall [8,9]. Blood flow velocities can increase locally by almost four orders of magnitude, from below approximately 0.01 mm/s in capillary vessels to greater than 500 mm/s in arterial vessels [10]. Furthermore, cardiovascular diseases are closely related to low magnitude shear stress including low shear stress (LSS), less than 5 dyn/cm^2, and oscillatory shear stress (OSS) in the artery. We recently reported that endothelial cells are amateur phagocytic cells for cell debris engulfment [11,12]. Furthermore, different flow stresses can influence the uptake of nanoparticles by endothelial cells [13]. Determining the relationship between vessel topology, local hemodynamics, and nanoparticle distribution will enable the selection of nanoparticles with higher specificity.

Peer review under responsibility of KeAi Communications Co., Ltd.
* Corresponding author.
** Corresponding author.
*** Corresponding author.
E-mail addresses: jhqiu@cqu.edu.cn (J. Qiu), wwewwy@163.com (Y. Wang), wanggx@cqu.edu.cn (G. Wang).
[1] These authors contribute equally.

https://doi.org/10.1016/j.bioactmat.2021.10.038
Received 9 August 2021; Received in revised form 11 October 2021; Accepted 20 October 2021
2452-199X/© 2021 The Authors. Publishing services by Elsevier B.V. on behalf of KeAi Communications Co. Ltd. This is an open access article under the CC BY-NC-ND license (http://creativecommons.org/licenses/by-nc-nd/4.0/).

Extracellular vesicles (EVs) are nanosized membranous vesicles produced by most kinds of cells [14]. They are enclosed by a lipid bilayer that surrounds an aqueous core containing proteins, lipids, and nucleic acids [15]. EVs are classified into exosomes, microvesicles, and apoptotic bodies on the basis of their biogenesis, release pathways, and sizes. EVs act as essential mediators to transfer bioactive molecules such as mRNAs, miRNAs, and proteins to target cells [16,17]. Given their ability to transfer bioactive components and surmount biological barriers, EVs are increasingly being explored as a potential therapeutic carrier for various applications [18]. However, to our best knowledge, the distribution of EVs in the blood vessels and the interaction between EVs and endothelial cells when they travel within the bloodstream are unclear.

Recently, red blood cell-derived EVs (RBCEVs) have been widely used as drug delivery carriers. Compared with EVs produced by other cells, RBCEVs are easier to prepare, safe, and have long circulation time [19,20]. Our previous research showed that the RBC-derived membrane-based drug delivery system is an excellent strategy for atherosclerosis therapy through intravascular administration [21]. Furthermore, RBCEVs are representative delegates for the distribution and engulfment of EVs in the blood flow because their membrane proteins have no specific targeting function. Therefore, we reasonably hypothesized that the uptake of RBCEVs by endothelial cells might also be affected by different flow patterns and shear stress. In this study, we used RBCEVs as the model of natural EVs to investigate the influence of hemodynamics on the interaction between EVs and endothelial cells *in vitro* and *in vivo*. The results showed that low magnitude shear stress increased the engulfment of RBCEVs by endothelial cells *in vitro* and *in vivo*, and LSS-induced endothelial cell oxidative stress is a regulator of EVs uptake (Fig. 1).

2. Materials and methods

2.1. Materials

1,19-Dioctadecyl-3,3,39,39-tetramethylindodicarbocyanine perchlorate (DiD) was purchased from Biotium Inc. (Fremont, USA). DAPI, cell total protein extraction kits, and *N*-acetyl-L-cysteine (NAC) were provided by Beyotime Institute of Biotechnology (Jiangsu, China). Antibodies against CD31 (ab28364) and Goat Anti-Rabbit IgG H&L (Alexa Fluor® 488) (ab150077) were obtained from Abcam. L-Ascorbic acid (VC) was purchased from Aladdin (Shanghai, China). Malondialdehyde (MDA), superoxide dismutase (SOD), and monocyte chemotactic protein 1 (MCP-1) enzyme-linked immunosorbent assay (ELISA) kits were provided by KeyGen Biotech (Nanjing, China).

2.2. RBCEVs derivation

RBCEVs were collected according to a previously reported method with some modifications [21]. Briefly, fresh whole blood was collected from male C57BL/6 mice (15–20 g) via orbital sinus puncture using EDTA spray-coated tubes (Labtub, China) and subsequently centrifuged at 600×*g* for 5 min at 4 °C (Centrifuge 5418 R, Eppendorf, Germany) to remove the plasma and white buffy coat. Then, the resulting packed RBCs were washed with 1 × PBS until the supernatant was clear. Next, RBCs were suspended in 0.25 × PBS containing 0.2 × 10^{-3} mol/L EDTAK2 for 30 min at 4 °C for hemolysis, and then the inner contents of RBCs were removed after centrifugation at 6500×*g* for 5 min. The resulting pellet was collected and washed three times with 1 × PBS. The collected RBC ghosts were resuspended in distilled water or saline. To obtain RBCEVs, RBC ghosts were frozen and thawed repeatedly for three times. Finally, RBC ghosts were extruded using an Avestin mini-extruder (Avestin, LF-1, Canada, 100 nm polycarbonate porous membrane) 10 times to harvest RBCEVs. The harvested RBCEVs were stored at 4 °C.

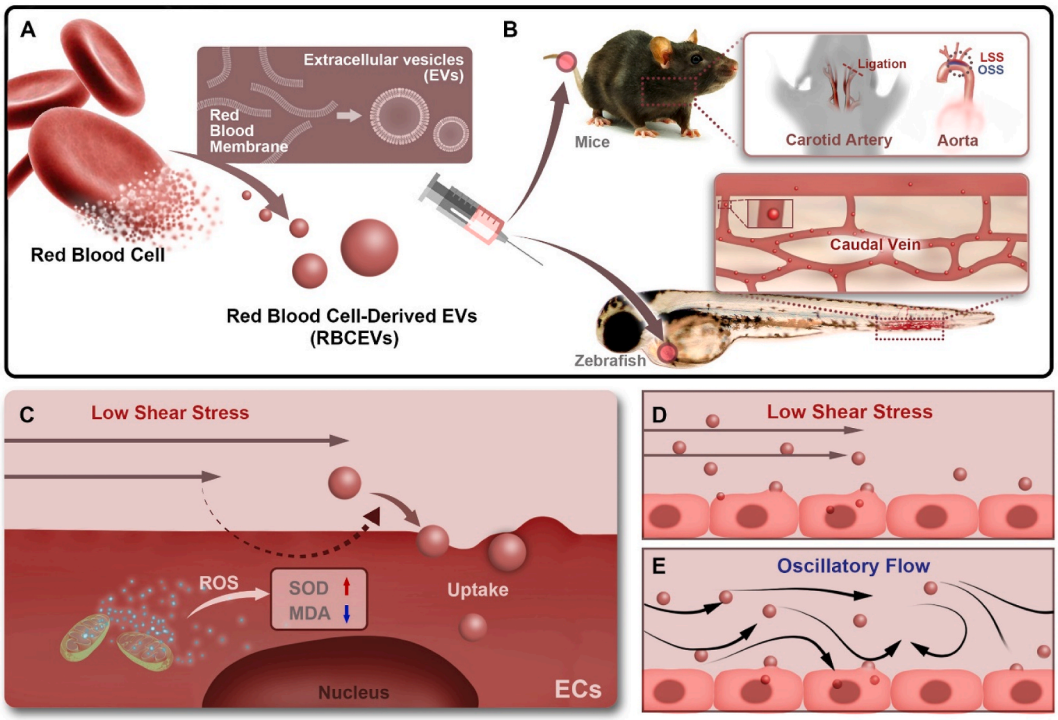

Fig. 1. Illustrations displaying that oxidative stress is involved in RBCEVs uptake by endothelial cells under low magnitude shear stress. (a) Preparation procedures of RBCEVs. (b) Low magnitude shear stress (LSS and OSS) promotes the uptake of RBCEVs by endothelial cells *in vivo*. (c–e) LSS-induced oxidative stress of endothelial cells is a regulator of EVs uptake.

2.3. DiD@RBCEVs

To prepare DiD@RBCEVs, RBC ghosts (from 200 μL of whole blood) after freeze and thaw were incubated with 1 μL of DiD (1 mg/mL) for 30 min. Then, they were centrifuged at 9500×*g* for 5 min at 4 °C and washed three times with 1 × PBS to remove free DiD. Next, DiD-labeled RBC ghosts were extruded with an Avestin mini extruder (Avestin, LF-1, Canada, 100 nm polycarbonate porous membrane) 10 times to obtain DiD@RBCEVs.

2.4. Characterization of RBCEVs

Analysis of zeta potential: The zeta potentials of RBCEVs and DiD@RBCEVs were determined using a Malvern Zetasizer Nano ZS unit (Nano ZS 90, Malvern, UK) with a He–Ne laser (λ = 633 nm) at a scattering angle of 90° at 25 °C.

Analysis of stability: The stability of RBCEVs and DiD@RBCEVs over a period of 48 h was evaluated in terms of particle size. The EVs maintained excellent stability with no significant change in particle size.

Transmission electron microscopy (TEM) analysis: The morphologies of RBCEVs and DiD@RBCEVs were observed by TEM at 200 kV (JEM-2100F, JEOL, Japan). To prepare the TEM samples, RBCEVs and DiD@RBCEVs suspension droplets were dripped on copper-coated mesh grids for 2 min and rinsed in filtered 1 × PBS. EVs on the grids were immediately fixed with 4% glutaraldehyde for 1 min and then negatively stained with 2% (wt/vol) Na phosphotungstate for 1 min.

Nanoparticle tracking analysis (NTA): We measured the size and concentration of EVs using NTA at VivaCell Biosceinces with ZetaView PMX 110 (Particle Metrix, Meerbusch, Germany) and corresponding software ZetaView 8.04.02. The isolated EVs samples were appropriately diluted using PBS buffer (Biological Industries, Israel) to measure the particle size and concentration. NTA measurement was recorded and analyzed at 11 positions. The ZetaView system was calibrated using 110 nm polystyrene particles. The temperature was maintained at around 25 °C. All samples were measured three times.

2.5. Characterization of membrane protein

The membrane proteins were identified by sodium dodecyl sulfate–polyacrylamide gel electrophoresis (SDS-PAGE). A total cell protein extraction kit (Beyotime) was used to extract the proteins of RBCEVs and RBC ghosts. The extracted proteins were run on 12% SDS-PAGE gel in a running buffer using a Bio-Rad electrophoresis system at 70 V for 0.5 h and then at 140 V for 1 h. Finally, the SDS-PAGE gel was stained with SimplyBlue. The expression of CD47 was detected by immunoblotting (WB). The lysate buffer containing 1% phosphatase inhibitor (Beyotime) was used to lyse RBCEVs, RBC ghosts, and RBC for 15 min at 4 °C. The lysis solution was centrifuged at 9500×*g* for 10 min at 4 °C. The supernatant was collected, and the protein concentration was determined by BCA protein analysis kit (Beyotime) [22]. The same amount of protein was separated from each sample with 12% SDS-PAGE and transferred to the polyvinylidene fluoride membrane (PVDF, Millipore, USA). The transferred PVDF membrane was sealed with 5% milk and then incubated with anti-CD47 primary antibody (anti-CD47 antibody, ab175388, Abcam) at 4 °C for 12 h. Finally, the PVDF membrane was incubated with HRP-coupled secondary antibody and observed by using a ChemiDoc-XRS imaging system (Bio-Rad).

2.6. Cell culture

HUVECs and brain endothelial cells were obtained from the Cell Bank of the Chinese Academy of Science (Shanghai, China). Cells were grown in RPMI-1640 medium containing 10% fetal bovine serum (FBS) at 37 °C in an atmosphere with 5% CO_2.

2.7. RBCEVs uptake by endothelial cells in vitro

Endothelial cells were seeded in 6-well plates at a density of 1×10^5 cells per well in 2 mL of RPMI-1640 medium containing 10% FBS and cultured at 37 °C with 5% CO_2 for 24 h. Before mechanical loading, endothelial cells were washed with a fresh culture medium and starved for 2 h. Then, they were placed on the corresponding mechanical equipment and treated with 50 μg/mL of RBCEVs for 3 h.

2.8. Shear stress treatment in vitro

Orbital shaker system: HUVECs were inoculated on standard 6-well plates in advance and incubated until the cells reached ~80% confluence. The 6-well plates were mounted on an orbital shaker and underwent a two-dimensional linear translation in the horizontal plane (i.e., XZ plane). Each well was filled with 2 mL of liquid medium. The orbital radius was 38 mm, and the orbital speeds were set to 162, 295, and 475 rpm to calculate the valuation of the shear stress in the cell well. Cells were cultured at 37 °C and 5% CO_2. The formula for the conversion between rotational speed and shear force is as follows:

$$\tau_\omega = a \times \sqrt{\rho \times u \times (2 \times \pi \times f)^3}$$

where τ_ω is shear stress, a is the orbital radius of rotation of the shaker, ρ is the density of the culture medium, u is the viscosity of the medium, and f is the frequency of rotation [23]. The shear stress in the cell well at 162 rpm, 295 rpm, and 475 rpm were about 5 dyn/cm^2 (LSS), 12 dyn/cm^2 (NSS), and 25 dyn/cm^2 (high shear stress, HSS), respectively. The Reynolds number was calculated as $\omega R^2/\nu$, where ω is the rotational speed of the orbital shaker, R is the radius of rotation of the cell well (13 mm), and ν is the kinematic viscosity ($1.012 \times 10^{-.6}$ m^2/s). The Reynolds number remained in the laminar regime.

Parallel-plate flow chamber: The cultured endothelial cells were subjected to shear stress in a parallel-plate flow chamber as described previously [24]. The formula $\tau = 6\ \mu Q/wh^2$ was used to calculate the fluid shear stress (τ), where Q is the flow rate and μ is the dynamic viscosity of the perfusate. The flow apparatus contained a peristaltic pump and an oscillatory pump (a frequency of 1 Hz and peak amplitude of 0.5 ± 4 dyn/cm^2) for OSS and only a peristaltic pump for LSS (5 dyn/cm^2), NSS (12 dyn/cm^2), and HSS (25 dyn/cm^2).

2.9. Labeling of lysosomes

The endothelial cells treated by DiD@RBCEVs were washed with 1 × PBS for three times and incubated with 50 nM LysoTracker red (Beyotime, China) for 1 h. Then, the cells were washed with 1 × PBS for three times before being stained with Hoechst 33342 (Beyotime, China). Lysosomes were viewed and counted, and the colocalization of lysosomes and EVs was examined by laser confocal microscopy.

2.10. Flow cytometry

1×10^5 HUVECs were inoculated on standard 6-well plates in advance and incubated with DiD@RBCEVs. Then, the cells were treated with different stresses for 3 h according to the requirements of the experiment. The cells were digested with trypsin. The cells were centrifuged at 150×*g* for 5 min and washed twice with 1 × PBS. Next, use a cell filter to the cell mass so that it is uniformly dispersed. Flow cytometry data were plotted and quantified using median fluorescence intensity (MFI) using in FlowJo software (Treestar, Ashland, USA).

2.11. Oxidative stress detection

Intracellular ROS production was evaluated with a ROS fluorescent probe CM-H2DCFDA (Genmed Scientifics, China). Briefly, after cell treatment, the cells/frozen sections were incubated with 10 μM CM-

H2DCFDA in PBS for 40 min in the dark at room temperature. Then, the cells/frozen sections were washed with 1 × PBS for three times before being stained with Hoechst 33342 and visualized under a laser confocal microscope.

Endothelial cells were seeded in 6-well plates. NAC (20 mM) and VC (10 mM) [25–27] were added to the culture medium, respectively. Then, the sample was placed on an orbital shaker system under LSS and NSS, respectively. After 1.5 h, RBCEVs were added and incubated for another 1.5 h. Endothelial cells were digested in trypsin. After centrifuging at 150×*g* for 10 min, the supernatants were removed and resuspended in 1 × PBS. Then, the samples were frozen and thawed three times at −20 °C. The upper supernatants were collected by centrifugation. The clear upper supernatants were collected for analysis of oxidative stress (MDA, SOD) and inflammatory factors (MCP-1). The concentrations of MDA, SOD, and MCP-1 were measured by ELISA kits according to the manufacturer's instructions (KeyGen Biotech, Nanjing, China).

2.12. Animal model

All animals received care according to the guidelines in the Guide for the Chongqing University Three Gorges Hospital, China. All animal care and experimental protocols were carried out with review and approval from the Laboratory Animal Welfare and Ethics Committee of Chongqing University Three Gorges Hospital (SYXK2017-0026).

Zebrafish model: All adult and larval zebrafish were grown according to guidance from China Zebrafish Resource Center. Zebrafish embryos expressing green fluorescent protein (GFP) in endothelial cells under the action of Flk1 promoter were collected. The GFP embryos in a Petri dish were collected without removing the chorion. After 24 h post-fertilization (hpf), the embryo was bathed in E3 standard fish liquid and treated with 0.003% phenylthiourea (St. Louis Sigma-Aldrich, Missouri Sigma-Aldrich) to prevent pigment formation. Zebrafish culture was carried out following the standard scheme [28]. Then, 48 hpf larvae were anesthetized with 0.2 mg/mL of tricaine methane (Sigma, USA) medium, and approximately 2 nL (50 μg/mL) of DiD@RBCEVs was injected into larval hearts. For imaging, the larval hearts were fixed on a 1% low melting point agarose (Thermo Fisher Science, Waltham, MA) and placed on a glass cover slide imaging dish (Mattek, Ashland, MA) at room temperature (24 °C). The images were obtained by using a laser confocal microscope at 1, 3, 6, and 12 h after injection. The blood flow velocities of arteries and veins of eight larvae were calculated.

Apoe$^{-/-}$ *mice model*: *Apoe*$^{-/-}$ mice in the C57BL/6 background were housed in a specific pathogen-free animal facility. Eight-week-old male *Apoe*$^{-/-}$ mice were fed a western diet under a strict 12 h light cycle for 8 weeks. For testing the biodistribution of RBCEVs, the mice were then randomly divided into three groups ($n = 8$) and injected with 150 μL of the following via the tail vein: (a) PBS, (b) DiD, and (c) DiD@RBCEVs. After injection 1 h, the mice were euthanized. Then, the aorta and organs were collected and washed three times with 1 × PBS to remove the blood. For observing the accumulation of RBCEVs in the plaque at different time points, the mice were randomly divided into three groups ($n = 3$), each group was injected with 150 μL DiD@RBCEVs. At different time points, the mice were euthanized. Then the aorta was collected and washed three times with 1 × PBS to remove the blood. The images and fluorescence quantification of the aorta and organs were performed using the *in vivo* small animal optical imaging system (Perkin Elmer) [29].

Partial ligation model: Eight-week-old male C57BL/6 mice were fed a normal chow diet under a strict 12 h light cycle. The mice were anesthetized with an intraperitoneal injection of pentobarbital sodium (1%, 40 mg/kg; Dainippon Pharmaceutical, Tokyo, Japan). The left carotid arteries (LCA) were separated using sterile surgical instruments. The external carotid artery (ECA), internal carotid artery (ICA), and occipital artery (OA) were ligated separately leaving blood flow only through the superior thyroid artery (STA). As the sham group (RCA), the contralateral right carotid arteries were separated but not ligated. After surgery, the mice were fed a chow diet under specific pathogen-free conditions until injection. After ligation, the mice were divided into three groups: (a) injection of 150 μL of PBS, DiD, or DiD@RBCEVs once; (b) injection of 150 μL of PBS, DiD, or DiD@RBCEVs daily for three consecutive days; and (c) injection of 150 μL of PBS, DiD, or DiD@RBCEVs daily for five consecutive days. The mice in each group were sacrificed 1 h after the last injection. Then, the LCA/RCA and organs were collected and washed three times with 1 × PBS to remove the blood. The images and fluorescence quantification of aorta and organs were performed using the *in vivo* small animal optical imaging system.

2.13. Oil red O staining

The aorta was stained with Oil Red O to evaluate the degree of atherosclerosis. Oil Red O staining was performed as previously described [30]. A stock Oil Red O solution (Sigma-Aldrich) was prepared by adding 150 mg of Oil Red O powder to 50 mL of isopropanol (Sigma-Aldrich). The aorta was fixed with 4% paraformaldehyde and then washed with 60% isopropanol. The aorta was stained for at least 1 h in a freshly diluted Oil Red O solution.

2.14. Immunofluorescence

The cells or frozen sections were washed with 1 × PBS three times, fixed in 4% paraformaldehyde for 15 min at room temperature, and washed three times. The cells or frozen sections were blocked in 5% bovine serum albumin for 1 h and then incubated overnight with CD31 antigen at 4 °C. On the second day, the cells or frozen sections were washed three times and incubated with fluorescence-coupled secondary antibodies for 2 h. The nuclei were stained with DAPI. The stained cells were imaged under a laser confocal microscope.

2.15. En face preparations and staining

Mice were euthanized and perfused with 0.9% saline. The LCA and RCA were harvested and fixed with 4% paraformaldehyde for 12 h on filter paper. Thereafter, the tissues were washed with Tris-buffered saline, and adventitia was removed. The luminal surfaces of the vessels were blocked with 5% bovine serum albumin before incubation with antigen CD31 diluted in blocker (1:100) for 1–2 nights at 4 °C. The following day, the vessels were washed and incubated with fluorochrome-conjugated secondary antibodies for 24 h. Samples were counterstained with DAPI to show the cell nucleus and photographed using a laser confocal microscope.

2.16. Uptake ratio of RBCEVs

The uptake ratio of RBCEVs was calculated using the following equation: $a/b \times 100\%$, where a is the number of endothelial cells that uptake RBCEVs and b is the number of total endothelial cells.

2.17. Statistical analysis

Statistical analyses were performed with Statistical Package for Social Sciences. Data are presented as mean ± SD. Experiments were performed with a minimum of three replications. Tukey's multiple comparison test, a Mann–Whitney *U* test, or a Student t-test was used to identify significant differences where appropriate. Significance is indicated as no significance (*ns*), or $P < 0.05$ (*), $P < 0.01$ (**), $P < 0.001$ (***). Imaris was used for data simulation and 3D reconstruction.

3. Results

Low magnitude shear stress promotes uptake of RBCEVs by endothelial cells *in vitro*. To confirm the characteristics of RBCEVs

uptake by endothelial cells, RBCEVs were first prepared and detected by NTA measurements and TEM. As shown in Fig. 2a and b, the NTA revealed the dominant peak in the particle size distribution between 110 nm and 120 nm for RBCEVs and DiD-labeled RBCEVs (DiD@RBCEVs), respectively. The ζ-potentials of RBCEVs and DiD@RBCEVs were −21 and −25 mV, respectively (Fig. 2c). In addition, SDS-PAGE protein analysis showed that RBCEVs and RBC ghosts were highly consistent in protein bands (Fig. 2d), and Western blot analysis showed that the functional protein CD47 also existed in RBCEVs (Fig. 2e). Furthermore, the TEM images showed that RBCEVs and DiD@RBCEVs displayed typical hollow vesicle structures of 80–100 nm (Fig. 2f and g). RBCEVs and DiD@RBCEVs maintained relative stability within 48 h (Supplementary Fig. 1). These results demonstrate the successful preparation of RBCEVs that were of similar size and structure to natural EVs.

To verify whether the uptake of RBCEVs by endothelial cells can be affected by different flow shears, the orbital shaker system was used to simulate various flow shear conditions [31]. The working principle of the orbital shaker system is shown in Fig. 3a. The shear stress

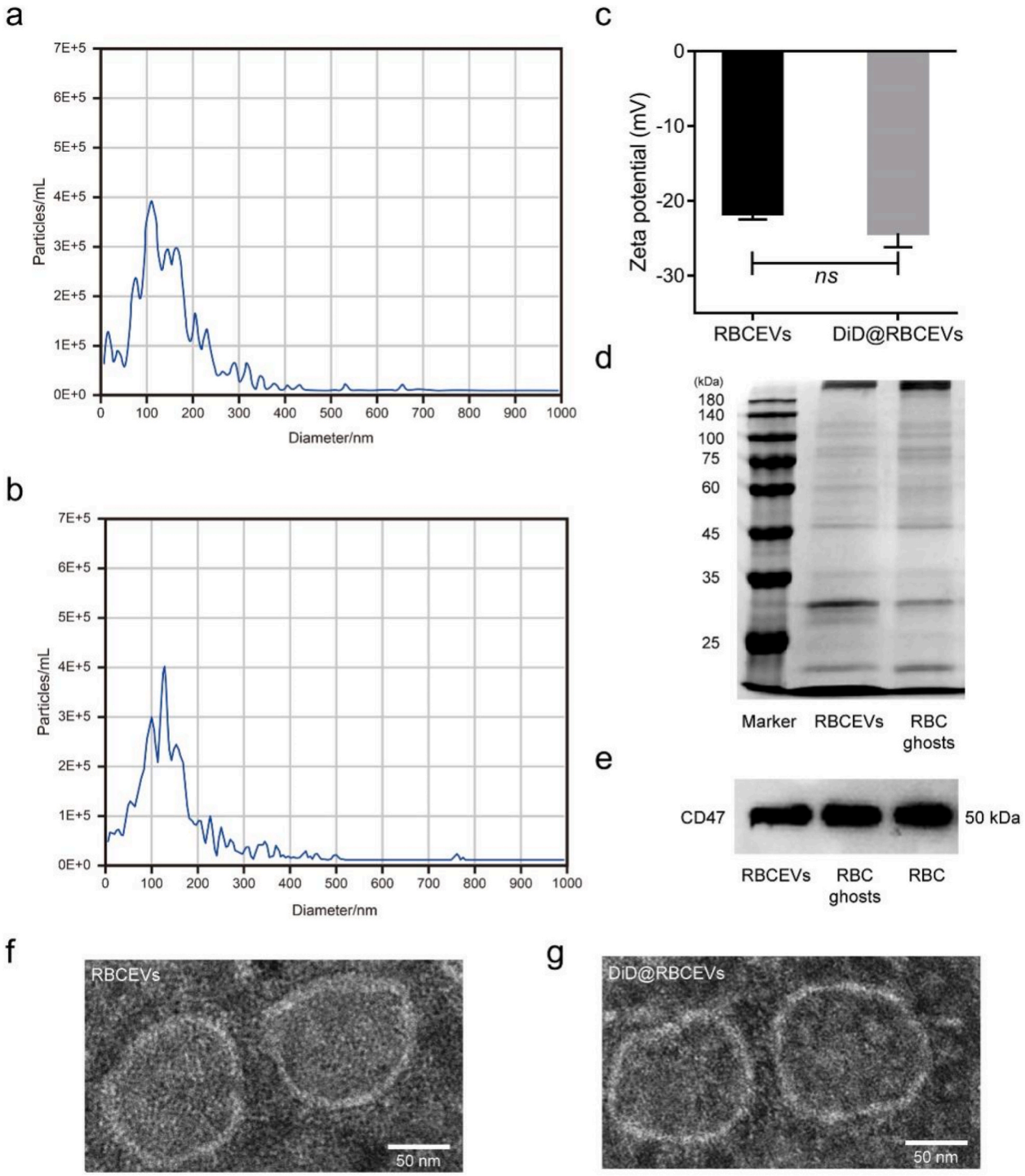

Fig. 2. Characterization of RBCEVs. (a–b) NTA of RBCEVs and DiD@RBCEVs. (c) Zeta potential of RBCEVs and DiD@RBCEVs. (d) Proteins in RBCEVs and RBC ghosts were characterized by SDS-PAGE. (e) Western blot analysis of CD47 in RBCEVs, RBC ghosts, and RBC. (f–g) TEM images of RBCEVs and DiD@RBCEVs. ($n = 3$) (scale bar = 50 nm). Significance is indicated as no significance (*ns*).

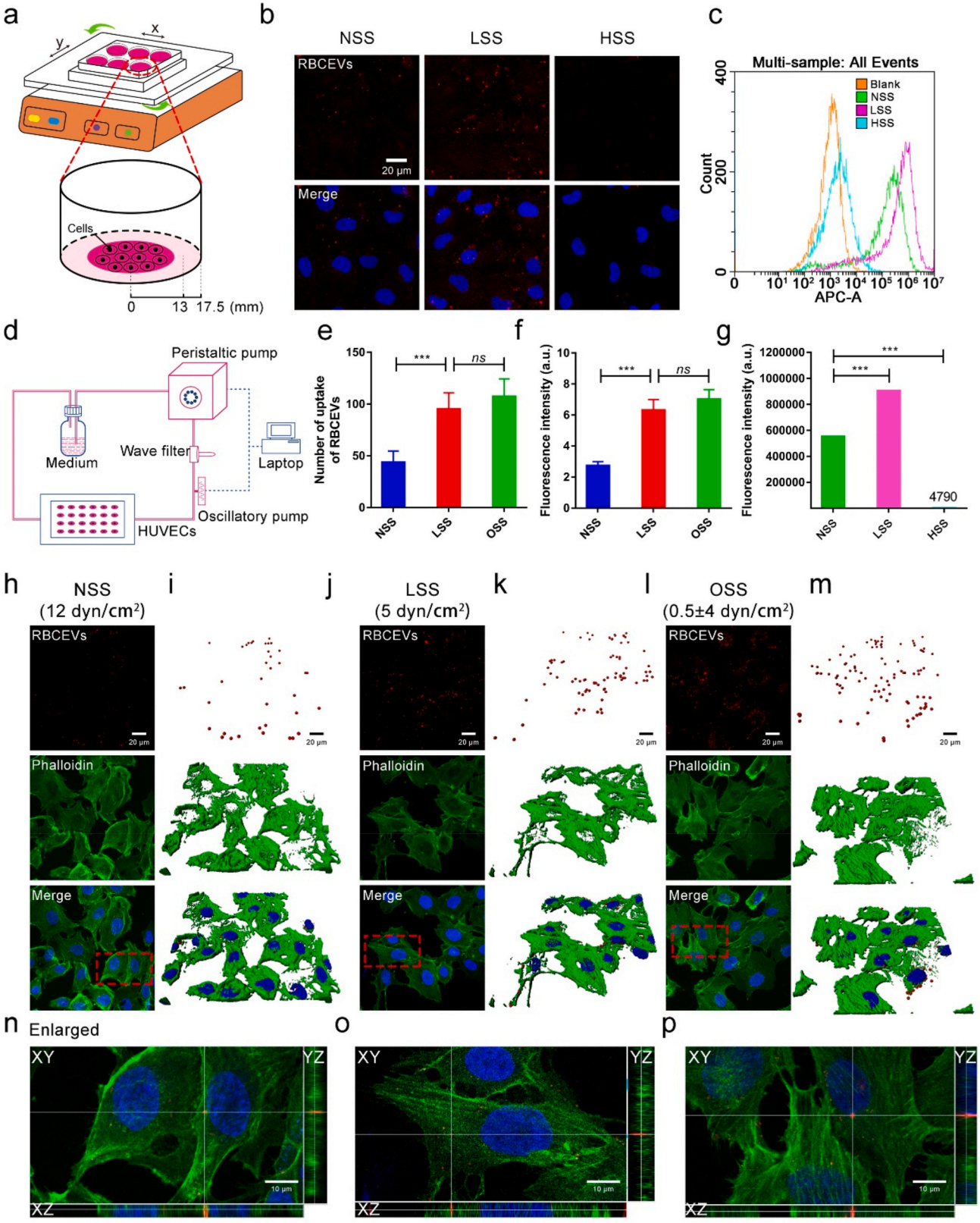

Fig. 3. Low magnitude shear stress promotes the uptake of RBCEVs by endothelial cells. (a) Model diagram of orbital shaker system. (b) Laser confocal images of RBCEVs that were uptake by endothelial cells at different shear stresses for 3 h. (c) and (g) Flow cytometry analysis of the uptake of RBCEVs by endothelial cells for 3 h. (d) Mechanical loading equipment model diagram of the parallel-plate flow chamber. (h), (j), and (l) Laser confocal images of RBCEVs that were uptake by endothelial cells under NSS, LSS, and OSS for 3 h. (i), (k), and (m) Imaris 3D rendering for (h), (j), and (l), respectively. (n), (o), and (p) XYZ axis showed uptake in different directions. (e) Quantitation of the number of RBCEVs uptake by endothelial cells and (f) mean fluorescence intensity of RBCEVs from (h), (j), and (l). ($n = 5$) (scale bar = 20 μm). Significance is indicated as no significance (*ns*), or $P < 0.001$ (***).

magnitudes in the center of the equipment can be changed by adjusting the rotational speed of the orbital shaker system according to the computational formula [23,32]. Using this equipment, the laser confocal images (Fig. 3b) showed that endothelial cells internalized RBCEVs in a shear stress-dependent manner. Under HSS, few RBCEVs were engulfed by endothelial cells. However, as the shear stress decreased, the uptake of RBCEVs by endothelial cells was gradually enhanced. Flow cytometry analysis further showed that the amount of RBCEVs uptake under LSS was increased by 1.67-fold and 189-fold compared with that under NSS and HSS, respectively (Fig. 3c and g). The endothelial cells have a complete cytoskeleton under NSS and HSS, indicating that the state of the cells is normal (Supplementary Fig. 2). Moreover, the uptake of RBCEVs by endothelial cells showed a time-dependent manner (Supplementary Fig. 3) and concentration-dependent manner (Supplementary Fig. 4) under the same shear stress. Meanwhile, the same phenomenon in which LSS induces RBCEVs engulfment was observed in the brain endothelial cells, another type of endothelial cells (Supplementary Fig. 5). These results indicate that LSS can enhance the uptake of RBCEVs. In addition, staining of lysosomes by LysoTracker (red fluorescence) revealed endolysosomal trafficking of most internalized RBCEVs in endothelial cells because the green RBCEVs and red lysosomes exhibited a high degree of colocalization under LSS (Supplementary Fig. 6).

Besides the varying levels of shear stress, different flow patterns are

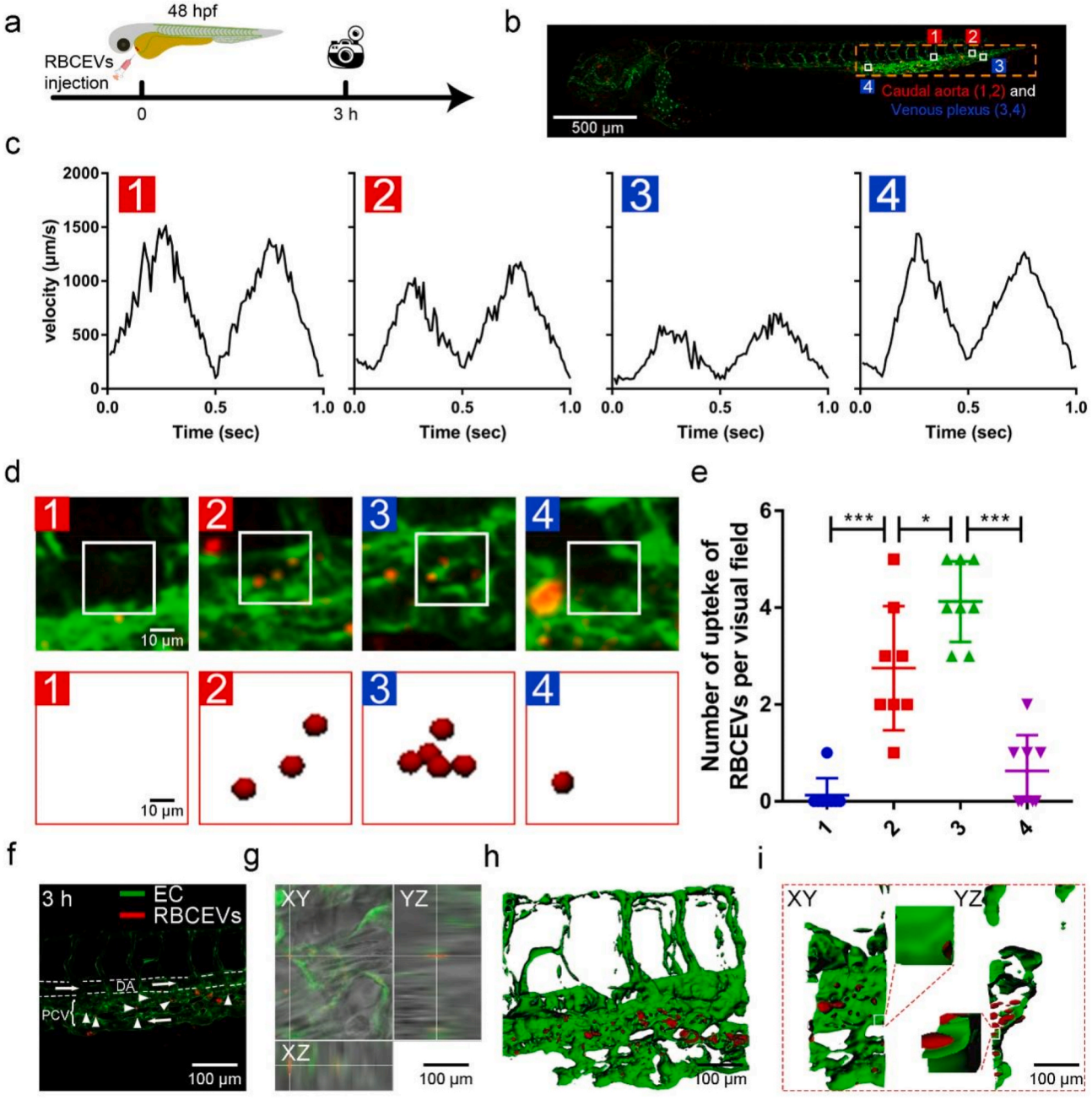

Fig. 4. Uptake of RBCEVs by endothelial cells at different blood flow velocities. (a) Images were taken with a laser confocal microscope. RBCEVs were injected into the heart. (b) Model diagram of zebrafish. (c) Blood flow velocities in the four different blood flow regions. (d) In the laser confocal image, the red puncta in the square represent RBCEVs at four speeds. (e) Number of RBCEVs uptake per visual field (scale bar = 500 μm). (f) In the laser confocal image, white arrows point to RBCEVs that were uptake by vascular endothelial cells at 3 h. (g) XYZ axis showed uptake in different directions. (h) Imaris 3D rendering and (i) front and lateral view *(n = 8)* (scale bar = 100 μm). Significance is indicated as $P < 0.05$ (*), or $P < 0.001$ (***).

also present in the dynamic environment of the bloodstream [33,34]. To investigate the influence of uptake under different flow patterns, the parallel-plate flow chamber that can mimic the flow dynamics of vascular bifurcation or straight arteries was used to evaluate the uptake of RBCEVs by endothelial cells under normal shear stress with laminar flow (NSS) and OSS, respectively (Fig. 3d). As shown in Fig. 3h–m, more RBCEVs were internalized by endothelial cells under OSS compared with NSS. Meanwhile, the *x-z* and *y-z* views showed that these engulfed RBCEVs were close to their perinuclear regions (Fig. 3n–p). The amount of RBCEVs uptake by endothelial cells under OSS was approximately 2-fold greater than that under NSS (Fig. 3e). Moreover, we repeated the endothelial cell uptake of RBCEVs under OSS, LSS, NSS, and HSS in the parallel-plate flow chamber. Consistent results were obtained with the orbital shaker system (Supplementary Fig. 7). In addition, the fluorescence intensity of RBCEVs uptake by endothelial cells under OSS was 3-fold brighter compared with that under NSS (Fig. 3f). Overall, these results demonstrate that low magnitude shear stress can promote the uptake of RBCEVs by endothelial cells.

LSS enhances the uptake of RBCEVs by endothelial cells in zebrafish. Zebrafish larvae are widely used in studying nanoparticle uptake due to their optical transparency and endothelial-specific fluorescence-labeled transgenic lines [35]. The blood flow velocity was evaluated by tracing the blood cells of zebrafish with a laser confocal microscope in endothelial-specific transgenic fish *Tg(flk:gfp)* (Fig. 4a). The results showed that the blood flow velocity in the dorsal aorta (DA) was Vmax = 1500 mm/s (position 1) and decreased to Vmax = 500 mm/s at the arteriovenous junction and caudal vein (positions 2–3, Fig. 4b and c). The above results showed that the caudal artery and posterior cardinal vein (PCV) have different blood flow velocities. Endothelial shear stress is proportional to blood viscosity. The calculation formula is endothelial shear stress = μ × dv/dy, where μ means blood viscosity, dv means blood velocity, and dy means radial distance from the wall [36].

To explore the effect of different blood flow velocities on the uptake of RBCEVs in zebrafish, DiD-labeled RBCEVs were microinjected into the heart of *Tg(flk:gfp)* zebrafish larva at 48 hpf, and the RBCEVs were traced by laser confocal microscopy at the tail. As shown by the white square (Fig. 4d), a multitude of RBCEVs aggregated at positions PCV 2 and 3, which were significantly more than 1 and 4 at the DA (Fig. 4e). RBCEVs were mainly uptake by endothelial cells in the PCV in the tail of zebrafish at 3 h (Fig. 4f and g). We also verified the distribution of RBCEVs at 6 and 12 h. RBCEVs were still present in the PCV at 12 h, which further indicated that the endothelial cells on PCV were the most important site for uptake of RBCEVs (Supplementary Fig. 8). Fluorescence images were further processed by Imaris (Fig. 4h and i) to reveal the details of RBCEVs uptake by endothelial cells. The *x-z* and *y-z* views of different cross-sections (Fig. 4h) and view of front and flank (Fig. 4i) demonstrated that the RBCEVs were co-located with green fluorescent endothelial cells and were prone to be engulfed in the area with a low blood flow velocity.

OSS induces uptake of RBCEVs by endothelial cells in mice. The partial ligation mouse model is a classical model to study the regulation mechanism of OSS [37,38]. The flow at ligated part of the left carotid artery (LCA) was disturbed flow with OSS [39,40], and the arrangement of cells was disordered. The unligated right carotid artery (RCA) was characterized with NSS, and the cells were aligned with the direction of blood flow. Therefore, we used the LCA ligation model of C57BL/6 mice to study the effects of OSS on the uptake RBCEVs by endothelial cells *in vivo*. The process diagram is shown in Fig. 5a and b. The fluorescence signals of RBCEVs in LCA and RCA were observed using a small animal optical imaging system. As illustrated in Fig. 5c and d, almost all the fluorescence appeared in the ligated parts. However, no apparent fluorescence signal was observed in the DiD fluorescence dye or PBS injected group. In addition, the fluorescence signal of the liver was obvious (Supplementary Fig. 9). Our finding is consistent with previous reports, wherein nanoparticles mainly accumulate in the liver, which are metabolized and eliminated [41].

To further observe the detail of RBCEVs uptake by endothelial cells, the *en face* staining and frozen section at the LCA and RCA were detected (Fig. 5e, h–i). Endothelial cells engulfed RBCEVs in the LCA. However, they did not engulf RBCEVs in the RCA, demonstrating that OSS was the main culprit of endothelial cells to engulf RBCEVs (Fig. 5f–g, h–i). The RBCEVs of LCA-5 d were significantly greater than those of LCA-1 d and LCA-3 d (Supplementary Fig. 10). Besides, we also found that endothelial cells engulfed the gold nanoparticles (Supplementary Fig. 11) and PLGA nanoparticles (Supplementary Fig. 12) under OSS *in vivo*. The *x-z* and *y-z* view and Imaris 3D rendering (Fig. 5e') indicated that RBCEVs were embedded between the nucleus and the cytoplasm and entered into the interior of the cells. These results further showed that OSS could promote the internalization of RBCEVs by endothelial cells *in vivo*.

High uptake of RBCEVs by endothelial cells in atherosclerotic lesions. Studies have confirmed that atherosclerotic (AS) plaques are prone to occur at low magnitude shear stress (LSS and OSS) areas [42,43]. To assess the effect of low magnitude shear stress on RBCEVs uptake under the cardiovascular disease model, *Apoe*$^{-/-}$ mice were fed with a high-fat diet for eight weeks followed by RBCEVs injection (Fig. 6a). Oil Red O staining was used to detect the formation of aortic plaques in *Apoe*$^{-/-}$ mice, which further proved the model's successful preparation (Fig. 6d). As shown in Fig. 6b and c, an intense fluorescence signal appeared in the aortic arch. The RBCEVs showed a marked increase compared with the other two control groups, indicating that RBCEVs were more likely to uptake by endothelial cells in the plaque area. Compared with the PBS and DiD groups, DiD@RBCEVs uptake was higher in endothelial cells of aortic plaques (Fig. 6e–i). We additionally found that even if injected once in *Apoe*$^{-/-}$ mice, RBCEVs could be detected at the plaque within 48 h (Supplementary Fig. 13). The fluorescence signals in visceral organs were also mainly accumulated in the liver (Supplementary Fig. 14). Taken together, the above results indicate that low magnitude shear stress could enhance the engulfment of RBCEVs by endothelial cells.

Oxidative stress is partially responsible for low magnitude shear stress-induced RBCEVs uptake by endothelial cells. To further explore how LSS mediated the uptake of RBCEVs by endothelial cells, endothelial cells were subjected to different treatments as shown in Fig. 7a. The results showed that endothelial cells treated with LSS all the time had the strongest uptake for RBCEVs (Fig. 7b–d), which is consistent with the finding that LSS may promote the aggregation of nanoparticles with the wall of the vessel and increase the time of contact between endothelial cells and nanoparticles [13]. Moreover, compared with endothelial cells treated with NSS all the time, endothelial cells pretreated with LSS could enhance the uptake of endothelial cells. The results indicate that the difference in uptake may be due to the changes in cell function and behavior under LSS.

It is well-known that LSS and OSS can induce oxidative stress and inflammation in cells [44,45]. Thus, intracellular ROS levels were detected with 6-chloromethyl-2′,7′-dichlorodihydrofluorescein diacetate, acetyl ester (CM-H2DCFDA) after different treatments (Fig. 7e). When endothelial cells were treated with NSS, LSS, and OSS for 3 h, respectively, the ROS of endothelial cells significantly increased under LSS and OSS (Fig. 7f). Similarly, compared with RCA, the ROS of LCA also significantly increased after carotid artery ligation in the mouse model (Fig. 7g and h). Next, we used an Enzyme-linked immunosorbent assay (ELISA) to detect the level of oxidative stress and inflammation in the supernatant of endothelial cells with or without LSS for 3 h. As shown in Fig. 7i, ELISA results showed that SOD protein level was increased and MDA protein level was decreased under LSS, while monocyte chemotactic protein 1 (MCP-1) protein expression level was not significantly changed, suggesting that oxidative stress can be rapidly induced by LSS. To elucidate whether the oxidative stress induced by LSS could mediate the uptake of endothelial cells for RBCEVs, we further added two general antioxidants L-ascorbic acid (VC) and *N*-acety-L-cysteine (NAC) to inhibit the production of intracellular ROS under LSS. We

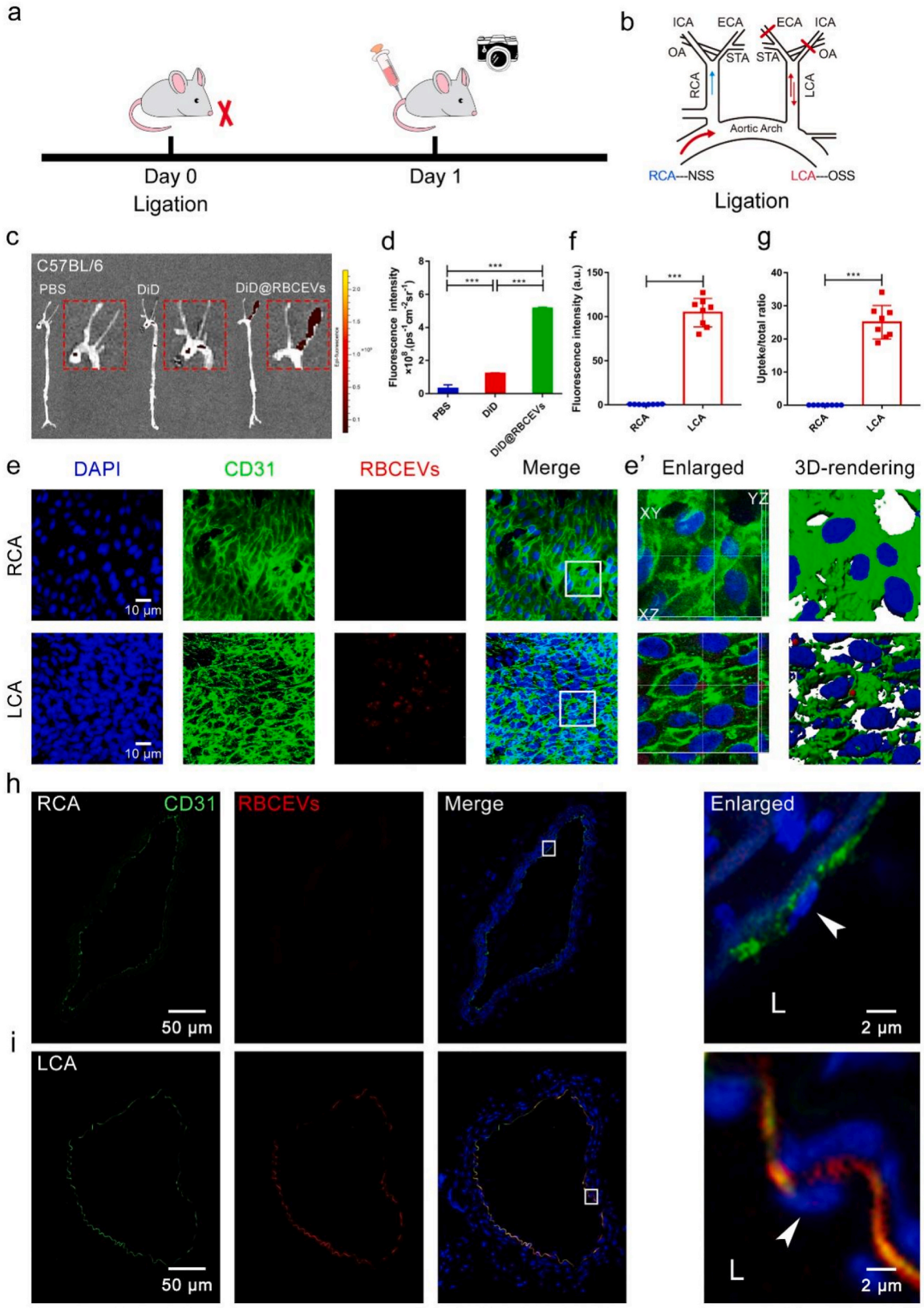

Fig. 5. OSS promotes the uptake of RBCEVs by endothelial cells in C57BL/6 mice. (a) Schematic of ligation establishment. (b) LCA of mice was ligated and immediately injected with DiD@RBCEVs. (c) Small animal optical imaging system. (d) Quantitative analysis of (c). (e) *En face* immunofluorescence images. OSS increased the uptake of RBCEVs by endothelial cells. (f) Quantitative analysis of mean fluorescence intensity and (g) uptake ratio. RCA: non-ligation; LCA: ligation for 1 day, injected once. The mice in each group were sacrificed 1 h after the last injection. (e') Imaris 3D rendering. ($n = 8$) (scale bar = 10 μm). (h–i) Immunofluorescence images and transection of the carotid artery. The white box indicates that the picture is locally enlarged, as indicated by the white arrow. LCA: ligation for 1 day, injection for 1 time, RCA: unligation. The mice in each group were sacrificed 1 h after the last injection. L: lumen. ($n = 8$) (scale bar = 50 μm). Significance is indicated as $P < 0.001$ (***).

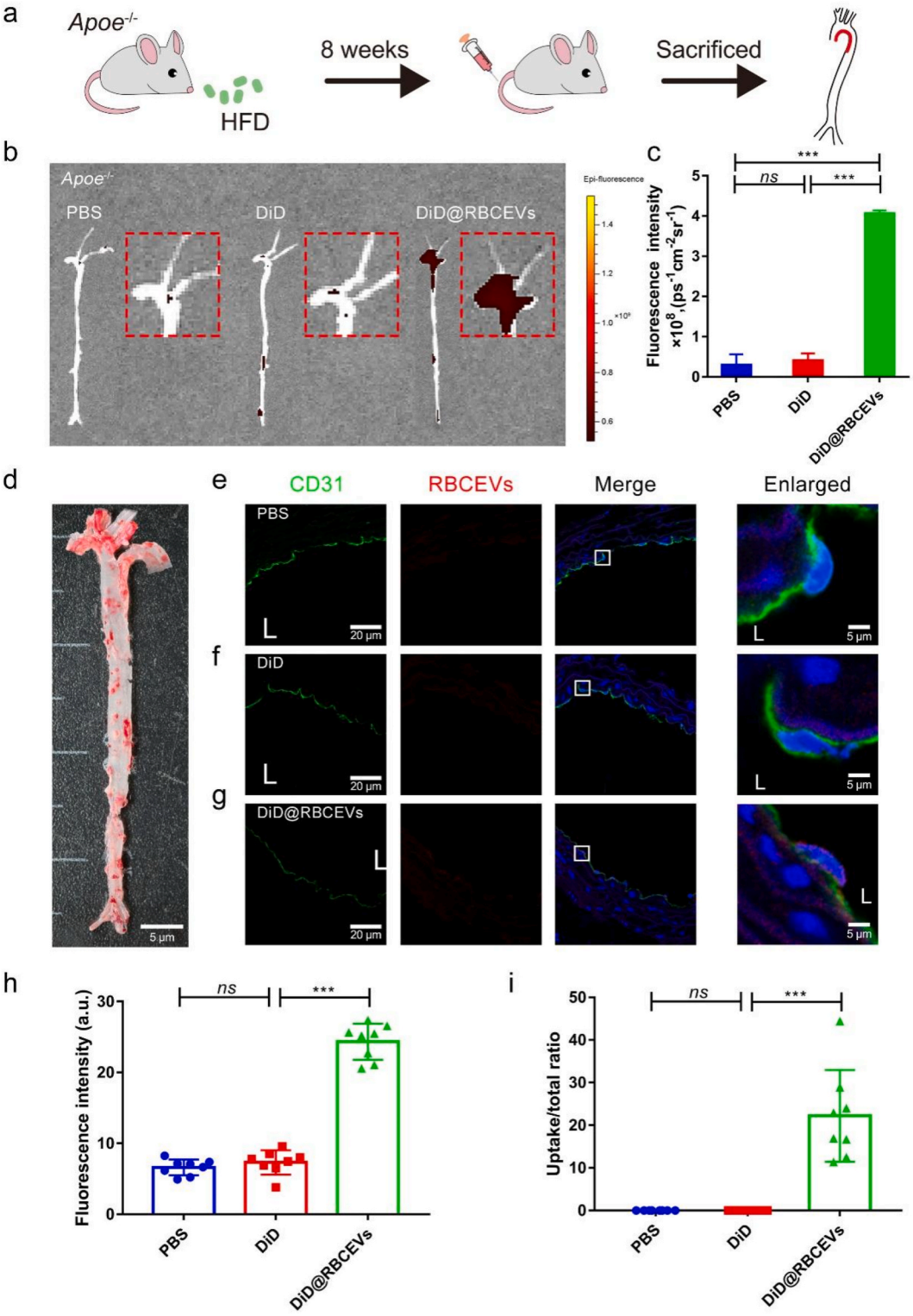

Fig. 6. Uptake of RBCEVs by endothelial cells in *Apoe*$^{-/-}$ mice. (a) Schematic of *Apoe*$^{-/-}$ mice. (b) Small animal optical imaging system. (c) Quantitative analysis of (b). (d) Oil Red O Staining on the total aorta. (e) to (g) Laser confocal images in the aorta. The white box indicates that the picture is locally enlarged, as indicated by the white arrow. (h) Quantitative analysis of mean fluorescence intensity and (i) uptake ratio. L: lumen. ($n = 8$) (scale bar = 20 μm) (scale bar = 5 μm). Significance is indicated as no significance (*ns*), or $P < 0.001$ (***).

found that the ROS of endothelial cells was alleviated, and the uptake efficiency of endothelial cells for RBCEVs decreased significantly after treatment with any of these antioxidants (Fig. 7j and k, Supplementary Fig. 15). Taken together, these results demonstrate that low magnitude shear stress can induce oxidative stress of endothelial cells and then increase uptake for RBCEVs.

4. Discussion

The biodistribution and uptake of nanoparticles by cells can

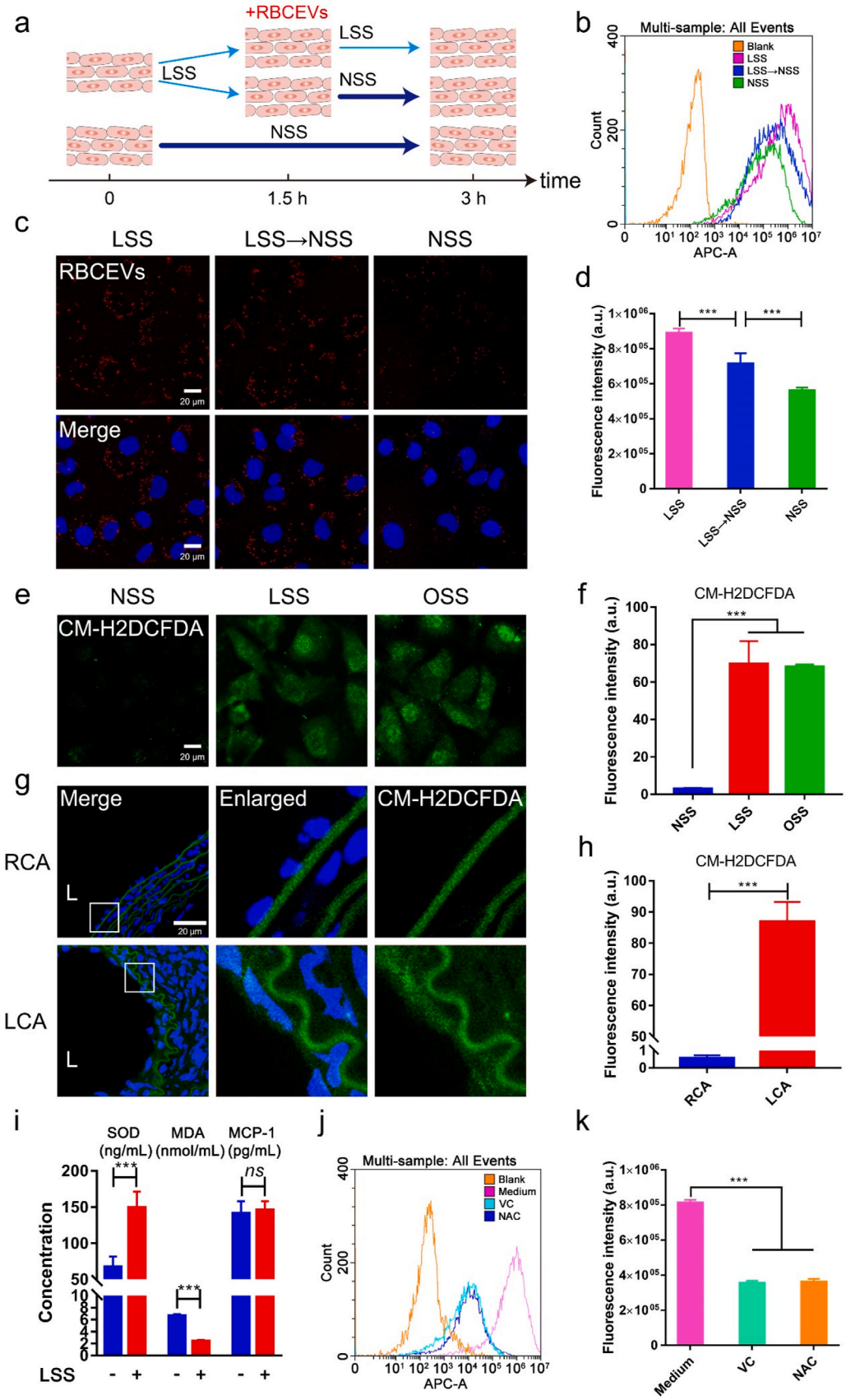

Fig. 7. Low magnitude shear stress-induced oxidative stress of endothelial cells was a regulator of RBCEVs uptake. (a) Model diagram of endothelial cells uptake in different shear stresses. (c) Laser confocal images of RBCEVs uptake by endothelial cells in different shear stresses. (b) and (d) Flow cytometry analysis for uptake of RBCEVs by endothelial cells in different shear stresses. (e–f) ROS production was measured by CM-H2DCFDA probe *in vitro*. (g–h) ROS production was measured by CM-H2DCFDA probe *in vivo*. (i) SOD, MDA, and MCP-1 levels were detected by an ELISA assay. (j–k) Flow cytometry analysis of RBCEVs uptake by endothelial cells treated with two antioxidants. L: lumen. ($n = 5$). Significance is indicated as no significance (*ns*), or $P < 0.001$ (***).

determine their therapeutic efficacy and toxicity *in vivo* [46–48]. In previous reports, the interaction of synthetic nanoparticles with cells and their distribution in the blood circulation system were well investigated *in vitro* cell experiments and some animal models [49,50]. However, few studies have investigated cell uptake in EVs under different flow patterns of the bloodstream. It has been reported that LSS (1.8 dyn/cm^2) can promote the uptake of synthetic nanoparticles by cells *in vitro*. After applying 10 dyn/cm^2, the uptake by cells decreased by 70% compared with LSS [51]. This finding indicated a strong nonlinear relationship between flow rate and nanoparticle uptake by cells. In addition, shear flow in governing the magnitude and feature of cell-nanoparticle interactions [52]. Unlike artificial synthetic nanoparticles, EVs are a kind of bilayer membrane vesicle of biological origin with good biocompatibility. Here, the uptake of RBCEVs by endothelial cells under different shear stresses was studied. We found that LSS can promote the uptake of RBCEVs by endothelial cells. Moreover, we confirmed that OSS can enhance the uptake of RBCEVs by endothelial cells. These findings indicate that flow patterns could influence the uptake of natural nanoparticles by cells.

We further established two animal models, including the visual zebrafish model and mouse carotid artery ligation model, to investigate RBCEVs uptake by endothelial cells *in vivo*. In the zebrafish model, the laser confocal real-time imaging and manual calculation showed that the velocity of PCV in the tail was only a third of that in DA, which was consistent with previous reports [53]. Subsequently, the uptake of fluorescent-labeled RBCEVs was observed by a laser confocal microscope. The results showed that RBCEVs were prone to be internalized by endothelial cells in slow-flow regions (LSS). Moreover, on the basis of the mouse carotid artery ligation model in our laboratory [28], which was previously built to research atherosclerosis formation on the basis of OSS in the vessel, we found that a large number of RBCEVs were deposited and uptake by endothelial cells in established OSS regions. In short, these results demonstrate that RBCEVs were preferentially internalized by endothelial cells *in vivo*, which may be due to the LSS or OSS increased the contact time of RBCEVs between endothelial cells. In AS mouse model, we confirmed that RBCEVs were prone to uptake by endothelial cells in the lesion areas. In addition to RBCEVs, we also verified the uptake of endothelial cells to solid nanoparticles such as gold nanoparticles and PLGA *in vivo*. The results showed that low magnitude shear stress could promote the uptake of nanoparticles by endothelial cells. We believe that the uptake of all kinds of nano-size particles could be uptake promoted by low magnitude shear stress. Therefore, this strategy can be used to guide or apply to the natural targeting mechanism of AS therapy.

Physical forces such as pressure and shear stress act as an oxidative stress inducer to cells [54]. We also found that low magnitude shear stress could promote the uptake of RBCEVs by endothelial cells due to oxidative stress rather than inflammation. The reason may be that the pro-inflammatory genes began to express later than oxidative stress genes [55]. Thus, oxidative stress was involved in the aggravation of uptake caused by low magnitude shear stress.

5. Conclusion

In this study, RBCEVs were used as a typical example of EVs to investigate the influence of EVs engulfment by hemodynamics and the amateur phagocytic potential of endothelial cells. Low magnitude shear stress (LSS and OSS) can increase the uptake of RBCEVs by endothelial cells *in vivo* and *in vitro*. Meanwhile, RBCEVs were preferentially internalized by endothelial cells in atherosclerotic plaque areas. Intriguingly, we found that oxidative stress induced by low magnitude shear stress acts as an accelerator to enhance endothelial cells uptake of RBCEVs. These findings also provide new mechanism and orientation for low magnitude shear stress-induced atherosclerosis development. We anticipate that this work will open a window onto biomechanics-related cell uptake and facilitate the development of therapeutic strategies for cardiovascular disease.

Author contributions

X.Q., K.Z., and J.Q. contributed equally to this work.

CRediT authorship contribution statement

Xian Qin: designed the research, conducted experiments, and analyzed data, Writing – original draft. **Kun Zhang:** designed the research, conducted experiments and analyzed data. **Juhui Qiu:** designed the research, Supervision, Writing – original draft. **Nan Wang:** conducted experiments and analyzed data. **Kai Qu:** conducted experiments and analyzed data. **Yuliang Cui:** conducted experiments and analyzed data. **Junli Huang:** conducted experiments and analyzed data. **Li Luo:** conducted experiments and analyzed data. **Yuan Zhong:** conducted experiments and analyzed data. **Tian Tian:** conducted experiments and analyzed data. **Wei Wu:** conducted experiments and analyzed data. **Yi Wang:** designed the research, Supervision, Writing – original draft. **Guixue Wang:** Funding acquisition, Resources, Project administration, Supervision, Conceptualization, Methodology, Visualization, Investigation.

Declaration of competing interest

There are no conflicts to declare.

Acknowledgment

This work was supported by the Key Project (12032007) and General Project (31971301, 31971242) of National Natural Science Foundation of China, the Chongqing Natural Science Foundation (cstc2019jcyj-zdxmX0028, cstc2019jcyj-xfkxX0004), and Fundamental Research Funds for Central Universities (2019CDYGZD008, 2019CDYGYB016, 2021CDJCGJ007). We gratefully thank the other staff of the Public Experiment Centre of State Bioindustrial Base (Chongqing) for providing technical support and assistance in data collection and analysis.

Appendix A. Supplementary data

Supplementary data to this article can be found online at https://doi.org/10.1016/j.bioactmat.2021.10.038.

References

[1] S.D. Perrault, W.C.W. Chan, In vivo assembly of nanoparticle components to improve targeted cancer imaging, Proc. Natl. Acad. Sci. U. S. A. 107 (2010) 11194–11199, https://doi.org/10.1073/pnas.1001367107.
[2] Y. Wang, K. Zhang, T. Li, A. Maruf, G. Wang, Macrophage membrane functionalized biomimetic nanoparticles for targeted anti-atherosclerosis applications, Theranostics 11 (2021) 164–180, https://doi.org/10.7150/thno.47841.
[3] J. Sun, Y. Zhu, L. Meng, T. Shi, X. Liu, Y. Zheng, A biodegradable coating based on self-assembled hybrid nanoparticles to control the performance of magnesium, Macromol. Chem. Phys. 216 (2015) 1952, https://doi.org/10.1002/macp.201500214, 1962.
[4] D. Zhu, I. Cockerill, Y. Su, Z. Zhang, J. Fu, K.E.W. Lee, J. Ma, C. Okpokwasili, L. Tang, Y. Zheng, Mechanical strength, biodegradation, and in vitro and in vivo biocompatibility of Zn biomaterials, ACS Appl. Mater. Interfaces 11 (2019) 6809–6819, https://doi.org/10.1021/acsami.8b20634.
[5] G. Morad, C.V. Carman, E.J. Hagedorn, J.R. Perlin, L.I. Zon, N. Mustafaoglu, T.-E. Park, D.E. Ingber, C.C. Daisy, M.A. Moses, Tumor-derived extracellular vesicles breach the intact blood–brain barrier via transcytosis, ACS Nano 13 (2019) 13853–13865, https://doi.org/10.1021/acsnano.9b04397.
[6] Maria E. Akerman, W.C.W. Chan, P. Laakkonen, S.N. Bhatia, E. Ruoslahti, Nanocrystal targeting in vivo, Proc. Natl. Acad. Sci. U. S. A. 99 (2002) 12617–12621, https://doi.org/10.1073/pnas.152463399.
[7] N. Korin, M. Kanapathipillai, B.D. Matthews, M. Crescente, A. Brill, T. Mammoto, K. Ghosh, S. Jurek, S.A. Bencherif, D. Bhatta, A.U. Coskun, C.L. Feldman, D. D. Wagner, D.E. Ingber, Shear-activated nanotherapeutics for drug targeting to obstructed blood vessels, Science 337 (2012) 738–742, https://doi.org/10.1126/science.1217815.

[8] J. Tan, S. Shah, A. Thomas, H.D. Ou-Yang, Y. Liu, The influence of size, shape and vessel geometry on nanoparticle distribution, Microfluid. Nanofluidics 14 (2013) 77–87, https://doi.org/10.1007/s10404-012-1024-5.

[9] O.F. Khan, M.V. Sefton, Endothelial cell behaviour within a microfluidic mimic of the flow channels of a modular tissue engineered construct, Biomed. Microdevices 13 (2011) 69–87, https://doi.org/10.1007/s10544-010-9472-8.

[10] G. Follain, D. Herrmann, S. Harlepp, V. Hyenne, N. Osmani, S.C. Warren, P. Timpson, J.G. Goetz, Fluids and their mechanics in tumour transit: shaping metastasis, Nat. Rev. Cancer 20 (2020) 107–124, https://doi.org/10.1038/s41568-019-0221-x.

[11] M.A.E.M. Sihombing, M. Safitri, T. Zhou, L. Wang, G. Wang, Unexpected role of nonimmune cells: amateur phagocytes, DNA Cell Biol. 40 (2020) 157–171, https://doi.org/10.1089/dna.2020.5647.

[12] T. Zhou, Y. Zheng, L. Sun, S.R. Badea, Y. Jin, Y. Liu, A.J. Rolfe, H. Sun, X. Wang, Z. Cheng, Z. Huang, N. Zhao, X. Sun, J. Li, J. Fan, C. Lee, T.L. Megraw, W. Wu, G. Wang, Y. Ren, Microvascular endothelial cells engulf myelin debris and promote macrophage recruitment and fibrosis after neural injury, Nat. Neurosci. 22 (2019) 421–435, https://doi.org/10.1038/s41593-018-0324-9.

[13] C.Y. Yang, A.M. Syed, P. MacMillan, J.V. Rocheleau, W.C.W. Chan, Flow rate affects nanoparticle uptake into endothelial cells, Adv. Mater. 32 (2020), 1906274, https://doi.org/10.1002/adma.201906274.

[14] J. Ding, G. Lu, W. Nie, L.-L. Huang, Y. Zhang, W. Fan, G. Wu, H. Liu, H.-Y. Xie, Self-activatable photo-extracellular vesicle for synergistic trimodal anticancer therapy, Adv. Mater. 33 (2021), 2005562, https://doi.org/10.1002/adma.202005562.

[15] N. Hamilton, N.M. Claudio, R.J. Armstrong, F. Pucci, Cell surface labeling by engineered extracellular vesicles, Adv. Biosyst. 4 (2020), 2000007, https://doi.org/10.1002/adbi.202000007.

[16] G. Fuhrmann, R. Chandrawati, P.A. Parmar, T.J. Keane, S.A. Maynard, S. Bertazzo, M.M. Stevens, Engineering extracellular vesicles with the tools of enzyme prodrug therapy, Adv. Mater. 30 (2018), 1706616, https://doi.org/10.1002/adma.201706616.

[17] M. Jarrige, E. Frank, E. Herardot, S. Martineau, A. Darle, M. Benabides, S. Domingues, O. Chose, W. Habeler, J. Lorant, C. Baldeschi, C. Martinat, C. Monville, L. Morizur, K. Ben M'Barek, The future of regenerative medicine: cell therapy using pluripotent stem cells and acellular therapies based on extracellular vesicles, Cells 10 (2021) 240, https://doi.org/10.3390/cells10020240.

[18] M.W. Schweiger, M. Li, A. Giovanazzi, R.L. Fleming, E. Tabet, I. Nakano, T. Wuerdinger, E.A. Chiocca, T. Tian, B.A. Tannous, Extracellular vesicles induce mesenchymal transition and therapeutic resistance in glioblastomas through NF-kappa B/STAT3 signaling, Adv. Biosyst. 4 (2020), 1900312, https://doi.org/10.1002/adbi.201900312.

[19] P.M. Glassman, C.H. Villa, A. Ukidve, Z. Zhao, P. Smith, S. Mitragotri, A.J. Russell, J.S. Brenner, V.R. Muzykantov, Vascular drug delivery using carrier red blood cells: focus on RBC surface loading and pharmacokinetics, Pharmaceutics 12 (2020) 440, https://doi.org/10.3390/pharmaceutics12050440.

[20] C.L. Modery-Pawlowski, L.L. Tian, V. Pan, A. Sen Gupta, Synthetic approaches to RBC mimicry and oxygen carrier systems, Biomacromolecules 14 (2013) 939–948, https://doi.org/10.1021/bm400074t.

[21] Y. Wang, K. Zhang, X. Qin, T. Li, J. Qiu, T. Yin, J. Huang, S. Mcginty, G. Pontrelli, J. Ren, Biomimetic nanotherapies: red blood cell based core–shell structured nanocomplexes for atherosclerosis management, Adv. Sci. 6 (2019), 1900172, https://doi.org/10.1002/advs.201900172.

[22] H. Cao, Z. Dan, X. He, Z. Zhang, H. Yu, Q. Yin, Y. Li, Liposomes coated with isolated macrophage membrane can target lung metastasis of breast cancer, ACS Nano 10 (2016) 7738–7748, https://doi.org/10.1021/acsnano.6b03148.

[23] K.T. Lim, J. Hexiu, J. Kim, H. Seonwoo, P.-H. Choung, J.H. Chung, Synergistic effects of orbital shear stress on in vitro growth and osteogenic differentiation of human alveolar bone-derived mesenchymal stem cells, BioMed Res. Int. (2014), 316803, https://doi.org/10.1155/2014/316803.

[24] K. Zhang, Y. Chen, T. Zhang, L. Huang, Y. Wang, T. Yin, J. Qiu, H. Gregersen, G. Wang, A novel role of Id1 in regulating oscillatory shear stress-mediated lipid uptake in endothelial cells, Ann. Biomed. Eng. 46 (2018) 849–863, https://doi.org/10.1007/s10439-018-2000-3.

[25] I. Johansson, V.T. Monsen, K. Pettersen, Jennifer Mildenberger, K. Misund, K. Kaarniranta, S. SchNberg, G. BjRkY, The marine n-3 PUFA DHA evokes cytoprotection against oxidative stress and protein misfolding by inducing autophagy and NFE2L2 in human retinal pigment epithelial cells, Autophagy (2015) 1636–1651, https://doi.org/10.1080/15548627.2015.1061170.

[26] C.Y. Chen, H. Yin, X. Chen, T.H. Chen, H.M. Liu, S.S. Rao, Y.J. Tan, Y.X. Qian, Y. W. Liu, X.K. Hu, M.J. Luo, Z.X. Wang, Z.Z. Liu, J. Cao, Z.H. He, B. Wu, T. Yue, Y. Y. Wang, K. Xia, Z.W. Luo, Y. Wang, W.Y. Situ, W.E. Liu, S.Y. Tang, H. Xie, Ångstrom-scale silver particle-embedded carbomer gel promotes wound healing by inhibiting bacterial colonization and inflammation, Sci. Adv. 6 (2020), eaba0942. https://doi: 10.1126/sciadv.aba0942.

[27] H. Tanaka, Y. Yamashita, K. Umezawa, T. Hirobe, S. Ito, K. Wakamatsu, The pro-oxidant activity of pheomelanin is significantly enhanced by UVA irradiation: benzothiazole moieties are more reactive than benzothiazine moieties, Int. J. Mol. Sci. 19 (2018) 2889, https://doi.org/10.3390/ijms 19102889.

[28] M.J. Gomez-Garcia, A.L. Doiron, R.R.M. Steele, H. Labouta, B. Vafadar, R. D. Shepherd, I.D. Gates, D.T. Cramb, S.J. Childs, K.D. Rinker, Nanoparticle localization in blood vessels: dependence on fluid shear stress, flow disturbances, and flow-induced changes in endothelial physiology, Nanoscale 10 (2018) 15249–15261, https://doi.org/10.1039/c8nr03440k.

[29] M. Krohn-Grimberghe, D. Von Elverfeldt, I. Neudorfer, K. Peter, M. Gawaz, C. H. Bode, C.V.Z. Muehlen, Development of a novel triple-target imaging strategy for the characterization of plaque inflammation in ApoE$^{-/-}$ mice, 976–976. Eur. Heart J. 34 (2013) https://doi.org/10.1093/eurheartj/eht310.P5360.

[30] Y. Huang, Y. Zheng, C. Jin, X. Li, L. Jia, W. Li, Long non-coding RNA H19 inhibits adipocyte differentiation of bone marrow mesenchymal stem cells through epigenetic modulation of histone deacetylases, Sci. Rep. 6 (2016), 28897, https://doi.org/10.1038/srep28897.

[31] N. Filipovic, K. Ghimire, I. Saveljic, Z. Milosevic, C. Ruegg, Computational modeling of shear forces and experimental validation of endothelial cell responses in an orbital well shaker system, Comput. Methods Biomech. Biomed. Eng. 19 (2015) 581–590, https://doi.org/10.1080/10255842.2015.1051973.

[32] J.M.D. Thomas, A. Chakraborty, M.K. Sharp, R.E. Berson, Spatial and temporal resolution of shear in an orbiting petri dish, Biotechnol. Prog. 27 (2011) 460–465, https://doi.org/10.1002/btpr.507.

[33] M. Harada, M. Ooki, K. Kohashi, T. Ichikawa, M. Kobayashi, Clinical survey of decreased blood flow rate in continuous renal replacement therapy: a retrospective observational study, Crit. Care Res. Pract. 20 (2019) 1–8, https://doi.org/10.1155/2019/2842313.

[34] N. Lucia, G. Claudia, C. Gergely, Y. Wei, M. Zhu, F.A. Di, H. Petra, Z. Ralf, S. Andreas, MIR-103 promotes endothelial maladaptation by targeting lncWDR59, Nat. Commun. 9 (2018), 2645, https://doi.org/10.1038/s41467-018-05065-z.

[35] V. Dóró, S.H. Jacobs, F.R. Hammond, H. Schipper, M. Forlenza, Visualizing trypanosomes in a vertebrate host reveals novel swimming behaviours, adaptations and attachment mechanisms, Elife 8 (2019), e48388, https://doi.org/10.7554/elife.48388.

[36] Y.S. Chatzizisis, A.U. Coskun, M. Jonas, E.R. Edelman, C.L. Feldman, P.H. Stone, Role of endothelial shear stress in the natural history of coronary atherosclerosis and vascular remodeling: molecular, cellular, and vascular behavior, J. Am. Coll. Cardiol. 49 (2007) 2379–2393, https://doi.org/10.1016/j.jacc.2007.02.059.

[37] L. Huang, D. Lei, W. Dong, C. Tang, G. Wang, Thrombosis model in mouse carotid induced by guidewire, J. Med. Biol. Eng. 36 (2016) 236–244, https://doi.org/10.1007/s40846-016-0125-0.

[38] A. Katsumi, A.W. Orr, E. Tzima, M.A. Schwartz, Integrins in mechanotransduction, J. Biol. Chem. 279 (2004) 12001–12004, https://doi.org/10.1074/jbc.R300038200.

[39] J. Zhou, P.-L. Lee, C.-S. Tsai, C.-I. Lee, T.-L. Yang, H.-S. Chuang, W.-W. Lin, T.-E. Lin, S.H. Lim, S.-Y. Wei, Y.-L. Chen, S. Chien, J.-J. Chiu, Force-specific activation of Smad1/5 regulates vascular endothelial cell cycle progression in response to disturbed flow, Proc. Natl. Acad. Sci. U. S. A. 109 (2012) 7770–7775, https://doi.org/10.1073/pnas.1205476109.

[40] C. Zhang, T. Zhou, Z. Chen, M. Yan, B. Li, H. Lv, C. Wang, S. Xiang, L. Shi, Y. Zhu, D. Ai, Coupling of integrin α5 to annexin A2 by flow drives endothelial activation, Circ. Res. 127 (2020) 1074–1090, https://doi.org/10.1161/CIRCRESAHA.120.316857.

[41] R. Deinzer, D. Hilpert, K. Bach, M. Schawacht, A. Herforth, Effects of academic stress on oral hygiene–a potential link between stress and plaque-associated disease? J. Clin. Periodontol. 28 (2010) 459–464, https://doi.org/10.1034/j.1600-051x.2001.028005459.x.

[42] F. Lin, L.J. Shaw, D.S. Berman, T.Q. Callister, J.W. Weinsaft, F.J. Wong, M. Szulc, V. Tandon, P.M. Okin, R.B. Devereux, J.K. Min, Multidetector computed tomography coronary artery plaque predictors of stress-induced myocardial ischemia by SPECT, Atherosclerosis 197 (2008) 700–709, https://doi.org/10.1016/j.atherosclerosis.2007.07.002.

[43] A.C. Akyildiz, L. Speelman, H.V. Brummelen, M.A. Gutiérrez, F.J. Gijsen, Effects of intima stiffness and plaque morphology on peak cap stress, Biomed. Eng. Online 10 (2011), https://doi.org/10.1186/1475-925X-10-25, 25–25.

[44] J. Chen, J. Zhang, J. Wu, S. Zhang, Y. Liang, B. Zhou, P. Wu, D. Wei, Low shear stress induced vascular endothelial cell pyroptosis by TET2/SDHB/ROS pathway, Free Radic. Biol. Med. 162 (2021) 582–591, https://doi.org/10.1016/j.freeradbiomed.2020.11.017.

[45] F. Vieceli Dalla Sega, G. Aquila, F. Fortini, M. Vaccarezza, P. Secchiero, P. Rizzo, G. Campo, Context-dependent function of ROS in the vascular endothelium: the role of the Notch pathway and shear stress, Biofactors 43 (2017) 475–485, https://doi.org/10.1002/biof.1359.

[46] A.P. Griset, J. Walpole, R. Liu, A. Gaffey, Y.L. Colson, M.W. Grinstaff, Expansile nanoparticles: synthesis, characterization, and in vivo efficacy of an acid-responsive polymeric drug delivery system, J. Am. Chem. Soc. 131 (2009) 2469–2471, https://doi.org/10.1021/ja807416t.

[47] Y. Fan, Y. Cui, W. Hao, M. Chen, Q. Liu, Y. Wang, M. Yang, Z. Li, W. Gong, S. Song, Y. Yang, C. Gao, Carrier-free highly drug-loaded biomimetic nanosuspensions encapsulated by cancer cell membrane based on homology and active targeting for the treatment of glioma, Bioact. Mater. 6 (2021) 4402–4414, https://doi.org/10.1016/j.bioactmat.2021.04.027.

[48] K. Abhange, A. Makler, Y. Wen, N. Ramnauth, W. Mao, W. Asghar, Y. Wan, Small extracellular vesicles in cancer, Bioact. Mater. 6 (2021) 3705–3743, https://doi.org/10.1016/j.bioactmat.2021.03.015.

[49] E. Connor, J. Mwamuka, A. Gole, C. Murphy, M. Wyatt, Gold nanoparticles are taken up by human cells but do not cause acute cytotoxicity, Small 1 (2010) 325–327, https://doi.org/10.1002/smll.200400093.

[50] D. Mahony, A.S. Cavallaro, F. Stahr, T.J. Mahony, S.Z. Qiao, N. Mitter, Mesoporous silica nanoparticles act as a self-adjuvant for ovalbumin model antigen in mice, Small 9 (2014) 3138–3146, https://doi.org/10.1002/smll.201300012.

[51] V. Charwat, I.O. Calvo, M. Rothbauer, S.R.A. Kratz, C. Jungreuthmayer, J. Zanghellini, J. Grillari, P. Ertl, Combinatorial in vitro and in silico approach to describe shear-force dependent uptake of nanoparticles in microfluidic vascular models, Anal. Chem. 90 (2018) 3651–3655, https://doi.org/10.1021/acs.analchem.7b04788.

[52] A. Tan, Y.Y. Lam, O. Pacot, A. Hawley, B.J. Boyd, Probing cell-nanoparticle (cubosome) interactions at the endothelial interface: do tissue dimension and flow matter? Biomater. Sci. 7 (2019) 3460–3470, https://doi.org/10.1039/c9bm00243j.

[53] G. Follain, Nal Osmani, A.S. Azevedo, G. Allio, J.G. Goetz, Hemodynamic forces tune the arrest, adhesion, and extravasation of circulating tumor cells, Dev. Cell 45 (2018) 33–52, https://doi.org/10.1016/j.devcel.2018.02.015, e12.

[54] N. Noriko, Role of oxidative stress in adaptive responses in special reference to atherogenesis, J. Clin. Biochem. Nutr. 43 (2008) 131–138, https://doi.org/10.3164/jcbn.2008068.

[55] N.E. Ajami, S. Gupta, M.R. Maurya, P. Nguyen, Y.S. Li, Y.J. Shyy, Z. Chen, C. Shu, S. Subramaniam, N.E. Ajami, Systems biology analysis of longitudinal functional response of endothelial cells to shear stress, Proc. Natl. Acad. Sci. U. S. A. 114 (2017), 10990, https://doi.org/10.1073/pnas.1707517114.